Aerospace Science and Technology 178 (2026) 112951

Contents lists available at ScienceDirect

Aerospace Science and Technology

journal homepage: www.elsevier.com/locate/aescte

Assessment of blade tip timing data from three novel bladed disk simulators based on a finite element modal model

Alhassan Nour [a], Philip Bonello [a,*], Peter Russhard [b], Mohamed Elsayed Mohamed [c], Pavel Procházka [d], Mohammed Lamine Mekhalfia [d]

[a] Department of Mechanical and Aerospace Engineering, University of Manchester, Manchester M13 9PL, United Kingdom
[b] EMTD Ltd, Derby DE72 3UX, United Kingdom
[c] School of Engineering and Computing, University of Lancashire, Preston PR1 2HE, United Kingdom
[d] Department of Dynamics and Vibration, Institute of Thermomechanics of the Czech Academy of Sciences, 18200, Prague, Czech Republic

ARTICLE INFO

Communicated by: Cummings Russell

Keywords:
Blade tip timing
Blade vibration
Bladed disk dynamics

ABSTRACT

The emergence of blade tip timing (BTT) data simulators, providing timing samples from their known blade tip vibration output, has been primarily driven by the necessity of developing and evaluating BTT signal processing algorithms, avoiding costly experimental set-ups. Apart from the realism required of its mathematical model, the simulator is required to produce data from all blades, and various configurations of probes, in feasible time frames, including the effect of axial deformation on the timing data. It should also have the capability to produce data with errors comparable to speed-dependent noise in real data. The novel contribution of this paper is the presentation of three novel bladed disk simulators that address these requirements, and their validation in a novel type of study that considers all blades of an aero-engine compressor, and which uses a commercial BTT software package to process the data and identify an excited blade mode-family member. Simulated data with speed-dependent errors amounting to 10% noise-to-signal ratio are successfully processed, resulting in mean errors of 2.4%, 0.15% in resonant amplitude and frequency across the blades. The simulated BTT data are shown to correctly distinguish between two excited mode-pair members differing by just 1% in natural frequency. Correlation with experimental BTT data is also presented.

1. Introduction

Turbomachinery blade vibration measurement has traditionally relied on strain gauges (SGs), but the use of such technology has declined over the last two decades in favour of blade tip timing (BTT) [1, 2]. Apart from disadvantages due to cost and complexity of installation (including telemetry), vulnerability to harsh operating environments, and interference with the structure and flow field [2], SGs suffer from the limitation of being unsuitable to monitor more than a few blades per rotor stage [1]. On the other hand, BTT is non-intrusive, is easy to install and durable, and enables the monitoring of all blades with a small number of sensors [2]. Compared to other non-contact methods, BTT supports flexibility in the selection of sensor type according to the requirements of the application [2].

The BTT process consists of a measurement system determining blade times of arrival (TOAs) from probes circumferentially distributed on the casing, and a signal processing algorithm to convert TOA data first to raw instantaneous displacement data (using their difference from the expected times of arrival [3]), and then to amplitude, frequency and phase for each blade in each revolution. The amplitude can then be converted to equivalent stress level using calibration factors based on finite element (FE) modelling [4]. The TOAs constitute what is termed as ‘BTT data’. The BTT instantaneous displacements derived from BTT data are inevitably under-sampled because the probes can only detect TOAs of a blade once per revolution, and the BTT signal processing algorithms are devised to deal with this feature [3].

BTT signal processing algorithms are extensively investigated in industry and literature, processing simulated and real BTT data [5]. The

Abbreviations: AD, angular differences; BTT, blade tip timing; CMM, coordinate measuring machine; CN, condition number; DOF, degrees of freedom; EO, engine order; FE, finite element; FRF, frequency response function; HP, high precision; LE, leading edge; ND, nodal diameter; NSR, noise-to-signal ratio; ODE, ordinary differential equation; OPR, once-per-revolution; PAD, product of angular differences; SG, strain gauge; TE, trailing edge; TOA, time of arrival.

* Corresponding author.
E-mail address: philip.bonello@manchester.ac.uk (P. Bonello).

https://doi.org/10.1016/j.ast.2026.112951
Received 8 December 2025; Received in revised form 22 April 2026; Accepted 17 June 2026
Available online 18 June 2026

emergence of BTT data simulators was primarily driven by the necessity of developing and evaluating BTT signal processing algorithms. BTT simulators allow for more accurate error estimation of the BTT process than experimental setups, provided that the simulated BTT data correlates well with real data, since the true (exact) vibration amplitude of resonance in simulations is known. BTT simulators avoid reliance on more costly experimental set-ups that would be required to generate BTT data and validate the process using alternative measurement systems (e.g. SGs). Additionally, BTT simulators can be used before such experimentation to ensure that an optimum experimental rig is set up, providing an assessment of detection capabilities of BTT systems applied for any type of vibration. BTT probe axial and radial position sensitivity can be evaluated before expensive design and casing modifications [5].

A BTT data simulator should generate accurate and realistic data to bridge the current gap between FE simulations and real BTT data. Most of the earlier BTT simulators presented in the literature were based on lumped parameter models (an idealised mass-spring-damper system representing each blade, coupled to its two neighbouring blades via two spring-damper systems linking adjacent blades), e.g. [6–9]. Several FE-based BTT simulators are available in the literature and have the potential to be more representative of real BTT data [3,10–13].

In this paper, three novel bladed disk simulators for generating BTT data based on FE reduced order modelling are presented and the reliability of their data is assessed in a novel type of study. The simulators determine BTT data from the time integrated mode superposition (reduced order model) solution for the bladed disk vibration (displacement time history data) similarly to [3,10–13], but the studies performed in the present paper use a much larger number of modes, to generate accurate time domain data predictions across the frequency range of interest. The three presented simulators differ from each other in the method of determination of the blade-probe crossing times (in the circumferential direction) of the FE nodes of interest on the blade tip, which is the first stage in determining the TOA of a blade at a probe. Two of the BTT simulators are termed 'interpolated TOA simulators' since the blade-probe crossing times are interpolated from the time-steps before and after the actual blade-probe crossing. To the authors' knowledge the use of interpolation to determine the blade-probe crossing times does not appear to have been previously verified. The third BTT simulator, is termed 'high precision TOA simulator', since the simulator relies on repeatedly increasing the time resolution in the vicinity of every blade-probe crossing point (by forcing reductions in the time step size) to generate highly precise blade-probe crossing times. Such a high-precision method of TOA determination was used previously in the simulators of [3,6–9,11,13,14] using the Matlab-Simulink block *Hit Crossing*. BTT data from the high-precision TOA simulator is used as a benchmark for the validation of the new interpolated TOA simulators. Simulation times using a high precision TOA simulator increase with the number of blades, number of probes and the magnitude of axial deformation (since this would require consideration of more FE nodes on the blade tip). On the other hand, simulation times for interpolated TOA simulators are independent of such factors. Accordingly, the use of interpolated TOA simulators, as opposed to the high precision TOA simulator, makes it feasible to generate BTT data for all blades and for many probes, which is necessary to allow for a proper assessment of BTT algorithms and to correlate simulated data with experimental data.

Real BTT displacement data contains instrumentation-induced noise, speed-independent offsets (e.g. probe positioning errors [15]), speed-dependent offsets (e.g. centrifugal forces, axial float, thermal expansion [15]) and speed-dependent fluctuations (additional noise) due to errors in TOAs and/or expected times of arrival, (Section 2.2) [16, 17]. Przysowa and Spychała in 2008 [18] were one of the first to discuss speed-dependent errors due to timing resolution of probes. He et al. [17] theorised and developed formulations to obtain speed-dependent errors in BTT displacement due to errors in the obtained TOAs and/or expected times, by isolating the effects of the probe's time resolution, vibration of probes and geometrical assumptions. Speed-dependent errors in BTT displacements are not usually observed when raw BTT displacements are presented in the literature, since instrumentation-induced noise is usually higher than the additional noise in the BTT displacement caused by the aforementioned speed-dependent errors [16]. However, improvements in BTT instrumentation will lead to reduced levels of instrumentation-induced noise, and the speed-dependent errors in BTT displacements will become apparent, as already evident in data presented in Wang et al. [19] in 2020, Ren et al. [20] in 2022 and Wang et al. [21] in 2022. Savitzky-Golay filtering [22] is typically used for minimising noise in BTT displacement data [3,21]. However, Savitzky-Golay filtering requires a BTT signal with a constant signal-to-noise ratio which would not provide optimum minimisation of speed-dependent errors in BTT displacements, as found in [21]. Minimisation of speed-dependent errors in BTT displacements requires adaptive filtering techniques, such as those utilised in industrial-grade commercial BTT software packages (e.g. [23], which is utilised in the present paper).

Although numerous researchers have taken highly precise simulated BTT displacement data and corrupted it with noise, speed-dependent offsets and speed-independent offsets (e.g. [6,24]), there have not been any attempts at generating simulated BTT data that result in speed-dependent errors in BTT displacements. For this reason, this paper considers two types of interpolated TOA simulators alongside the high precision (HP) TOA simulator. Whereas one of the interpolated TOA simulators will be shown to have comparable accuracy to the HP TOA simulator, the other performs blade-probe crossing time interpolation in such a way as to induce speed-dependent errors in the BTT displacement data.

Apart from the novel aforementioned interpolation for blade-probe crossing times, all three simulators utilise a novel axial interpolation method which considers the effect of axial deformation to accurately determine the TOA at a probe from the blade-probe crossing times of the various FE nodes of the blade tip (second and final stage in TOA determination). As will be shown in the present paper, this method overcomes the hitherto unreported problem of discontinuities in BTT displacement data introduced by the discrete FE nodes on the blade tip in FE-based BTT simulators. The method ensures that the TOA pertains to the point on the blade tip that is actually detected by the probe (i.e. the point that is instantaneously coincident with the axial position of the probe, in addition to being circumferentially coincident), rather than the nominal sensing point or any other point on the blade tip. Hence, the sampled displacements derived from such TOAs simulate the BTT displacements obtained in real-world applications. Such displacements are different from the tangential displacements of the nominal sensing point [4], which is what would be obtained if the TOAs are based only on this point. Previous simulation work, e.g. [3,11–13], did not consider or report the problems introduced by axial deformation that are reported and resolved in the present paper. The reason for this was either that the TOAs were based on the nominal sensing point on the blade tip (as in fact stated in Fig. 18 of [3]), or because the displacement samples were determined using an approach that did not use the difference between the actual and expected arrival times [11,13]. As discussed in Section 2.1, this latter approach does not follow the real-world BTT process, despite taking into account the deviations of the nominal sensing point from the axial position of the probe.

The reliability of the BTT data generated by the aforementioned novel simulators is validated in a study that is novel in three aspects: (i) it considers BTT data from all blades of the FE-based model of an aero-engine compressor; (ii) it introduces an equivalent BTT displacement time function based on the nominal sensing point as an independent benchmark for validation; (iii) the BTT data (arrival times) generated by the simulators are validated by feeding them into a commercial BTT software package (MultiTool [23]), whose output for amplitude and frequency is then correlated with the equivalent BTT displacement time function from the simulator for determination of BTT errors. The excitation type used in the simulators is a harmonic travelling wave excitation that is phased to excite modes of a given number of nodal diameters (N_{ND}) within a blade-dominated mode family, as in [25].

2. BTT data simulator and analysis methodology

2.1. BTT displacement definition and benchmarking

The BTT probes are axially positioned to detect blade arrival at a particular area of interest on a blade tip, e.g. trailing edge (TE) or leading edge (LE). With reference to Fig. 1, probe no j has a fixed position at $\left(x_j, y_j,\ z_j\right)$ and its angular position is $\theta = \theta_j$. The point on a blade that has the same axial position as the probe when the blade is undeformed is defined as the nominal sensing position $\mathrm{P_{nom}}$ on the blade i.e. $z_{\mathrm{P_{nom}}}|_{\mathrm{undef}} = z_j$. In this work, the FE model has a node corresponding to $\mathrm{P_{nom}}$. The BTT displacement detected by probe no j is determined from the difference between the expected time of arrival of the blade (i.e. the time based solely on rotation of the undeformed blade), $t_{\exp,j,\mathrm{P_{nom}}}$, and the actual time of arrival, $t_{\mathrm{TOA},j}$:

$$d_j = \Omega R^{(\mathrm{ref})}_{\mathrm{P_{nom}}}\left(t_{\exp,j,\mathrm{P_{nom}}} - t_{\mathrm{TOA},j}\right) \tag{1}$$

where $R^{(\mathrm{ref})}_{\mathrm{P_{nom}}}$ is the radius at $\mathrm{P_{nom}}$ and Ω is the average rotational speed over one revolution. In this work, $t_{\exp,j,\mathrm{P_{nom}}}$ is obtained directly from the times of angular coincidence of $\mathrm{P_{nom}}$ with the probe position, assuming rigid body motion. This eliminates errors in $t_{\exp,j,\mathrm{P_{nom}}}$, which are typically obtained using a once-per-revolution (OPR) probe [24,26].

With regard to the actual arrival times of the blade $t_{\mathrm{TOA},j}$, these will generally not pertain to $\mathrm{P_{nom}}$ due to the axial deformation, as shown in Fig. 1, and will be determined using the method in Section 2.2 (including axial interpolation between the FE nodes $P_{k_{\min,1}}$ and $P_{k_{\min,2}}$). However, as seen from Fig. 1, d_j can be related to the axial and tangential displacements of $\mathrm{P_{nom}}$ at $t = t_{\mathrm{TOA},j}$ (relative to its undeformed location), denoted as $d_{z,j}$, $d_{\mathrm{tang},j}$ respectively, using the following relation:

$$d_j = d_{\mathrm{tang},j} + d_{z,j}/\tan(\eta_{\mathrm{tip}}) \tag{2}$$

For the present rotor, the angle η_{tip} is 41.5°. In general, defining an equivalent BTT displacement function in the time domain, $d_{\mathrm{eqv}}(t)$:

$$d_{\mathrm{eqv}}(t) = d_{\mathrm{tang}}(t) + d_z(t)/\tan(\eta_{\mathrm{tip}}) \tag{3}$$

where $d_z(t)$, $d_{\mathrm{tang}}(t)$ are the instantaneous axial and tangential displacements of $\mathrm{P_{nom}}$, we can say from the previous two equations that

$$d_j = d_{\mathrm{eqv}}\left(t_{\mathrm{TOA},j}\right) = d_{\mathrm{tang}}\left(t_{\mathrm{TOA},j}\right) + d_z\left(t_{\mathrm{TOA},j}\right)/\tan(\eta_{\mathrm{tip}}) \tag{4}$$

since, by definition in Fig. 1, $d_{\mathrm{tang},j} = d_{\mathrm{tang}}\left(t_{\mathrm{TOA},j}\right)$, $d_{z,j} = d_z\left(t_{\mathrm{TOA},j}\right)$. In the present paper $d_{\mathrm{eqv}}(t)$ is used to benchmark the accuracy of the amplitude and displacement derived from the independently determined BTT data.

It should be noted that the above relations Eqs. (2)–(4) assume a very thin blade tip and neglect the error from any twisting deformation $\delta\eta_{\mathrm{tip}}$ (including blade untwist). The latter is justified by considering that such an error would be a second order effect i.e. $O\{d_z \cdot \delta\eta_{\mathrm{tip}}\}$.

It is important to note that, despite the evident equivalence of d_j and $d_{\mathrm{eqv}}\left(t_{\mathrm{TOA},j}\right)$ (which is verified in Section 3.2), the BTT displacement data d_j is (and should be) always determined independently of $d_{\mathrm{eqv}}(t)$ using Eq. (1) rather than the samples of $d_{\mathrm{eqv}}(t)$ at $t = t_{\mathrm{TOA},j}$. The reasons for this are twofold:

- it ensures independent benchmarking (via $d_{\mathrm{eqv}}(t)$) for the simulated BTT process;
- BTT probes can only measure TOAs, which means that Eq. (1) cannot be avoided in practice, and commercial BTT software packages typically take such TOAs as inputs (e.g. [23]).

It is noted that recent BTT simulator work [11,13] has avoided using Eq. (1) by considering the BTT displacement as the tangential deflection of the node on the blade tip that comes closest axially to the probe at the instant it crosses the probe's angular position. However, from Fig. 1 it is seen that such a deflection is not actually equal to the (true) BTT displacement d_j (Eq. (1)) or its equivalent $d_{\mathrm{eqv}}\left(t_{\mathrm{TOA},j}\right)$. Hence, in addition to missing the features bulleted above, the simulated BTT displacement data extraction method in [11,13] is not aligned with BTT practice. The motivation for not using Eq. (1) in [11,13] was to avoid use of an average rotational speed over each revolution to calculate the BTT displacement under variable speed conditions or speed fluctuation [11]. However, speed fluctuations should be smoothed out before applying Eq. (1), and this fundamental BTT relation worked well in [3] (where angular velocity sweeps of 100 rev/s in 1 s were considered). Also, Eq. (4) provides an independent check for Eq. (1).

2.2. Determination of times of arrival by the simulator

Let $\left(R^{(\mathrm{ref})}_{\mathrm{P}_k},\ \theta^{(\mathrm{ref})}_{\mathrm{P}_k}\right)$, where $0 < \theta^{(\mathrm{ref})}_{\mathrm{P}_k} \le 2\pi$, be the x-y plane polar coordinates corresponding to the Cartesian coordinates $(x^{(\mathrm{ref})}_{\mathrm{P}_k}, y^{(\mathrm{ref})}_{\mathrm{P}_k}, z^{(\mathrm{ref})}_{\mathrm{P}_k})$ of a blade tip node P_k ($k = 1, \ldots K$) in a reference angular position of the undeformed bladed disk at which $t = 0$. Neglecting shaft vibration, the angular position of P_k at time t, $\theta_{\mathrm{P}_k}(t)$, is given by superimposing the angular deformation $\delta\theta^{(\mathrm{def})}_{\mathrm{P}_k}(t)$ relative to a rotating x-y frame, onto the angular position of P_k under rigid conditions $\theta^{(\mathrm{rgd})}_{\mathrm{P}_k}(t)$, and "flooring" the result to the range $(0, 2\pi]$ [3]. The deformation $\delta\theta^{(\mathrm{def})}_{\mathrm{P}_k}(t)$ is calculated

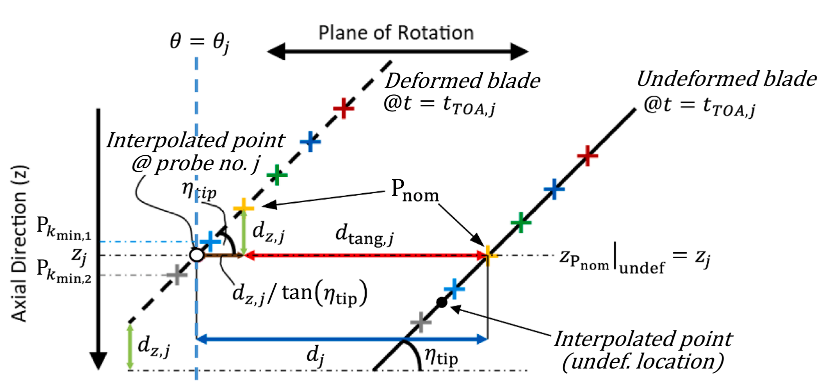

Fig. 1. Axial and tangential deflections of nominal sensing point $\mathrm{P_{nom}}$ (depicted as a yellow '+') on a blade tip (including FE nodes) at the instant of arrival of the blade tip at probe no j i.e. $t = t_{\mathrm{TOA},j}$.

from the deformation displacements $\delta x_{P_k}^{(def)}$, $\delta y_{P_k}^{(def)}$, $\delta z_{P_k}^{(def)}$ of P_k in the rotating x-y frame, which are determined by mode superposition of the time-integrated solution of the modal equations of motion of the bladed disk assembly under excitation $\mathbf{f}(t)$ [3]. The excitation force $\mathbf{f}(t)$ on the blade-disk assembly is a superposition of M chirp signals with user prescribed fixed engine orders (EOs):

$$\mathbf{f}(t) = \left[\cdots F_{x_{Qn}}(t)\ F_{y_{Qn}}(t)\ F_{z_{Qn}}(t)\ \cdots\right]^T \tag{5}$$

where, for example, $F_{z_{Qn}}^{(m)}$ represents the z-directional dynamic excitation force for nodes Q_n $(n = 1,\ \dots,\ N)$ due to an EO_m excitation:

$$F_{z_{Qn}}(t) = \sum_{m=1}^{M} F_{z_{Qn}}^{(m)}(t) = \sum_{m=1}^{M} A_{z_{Qn}}^{(m)} \sin\left[EO_m\left(\Omega_i t + \left(\frac{\Omega_f - \Omega_i}{2T_s}\right)t^2\right) + \varphi_{z_{Qn}}^{(m)}\right] \tag{6}$$

For a travelling wave, $\varphi_{z_{Qn}}^{(m)}$ is:

$$\varphi_{z_{Qn}}^{(m)} = \frac{2\pi(b-1)N_{ND}}{N_b} \tag{7}$$

where $b = 1,\ 2, \dots,\ N_b$ is the blade number corresponding to node Q_n. N_b is the total number of blades and N_{ND} is the user prescribed number of nodal diameters.

With reference to Fig. 1, $t_{TOA,j}$ is determined in two stages A, B:

A. Detection of the crossing times t_{det,j,P_k} at which all blade tip nodes of interest, P_k $(k = 1, \dots K)$, cross the angular position of the probe no j, θ_j, by solving the equation

$$\theta_{P_k}\left(t_{det,j,P_k}\right) - \theta_j = 0 \tag{8}$$

B. Determination of $t_{TOA,j}$ from $t_{det,j,P_k}(k = 1, \dots K)$, through a novel approach that interpolates between the two FE nodes $P_{k_{min,1}}$ and $P_{k_{min,2}}$ that are axially positioned nearest to probe no j. $(z = z_j)$ and on opposite sides of it, at their respective crossing times $t = t_{det,j,P_{k_{min,1}}}$, $t = t_{det,j,P_{k_{min,2}}}$.

With regard to stage B, the TOA is determined as follows.

$$t_{TOA,j} = t_{det,j,P_{k_{min,1}}} - \Delta z_{j,P_{k_{min,1}}}\left(\frac{t_{det,j,P_{k_{min,2}}} - t_{det,j,P_{k_{min,1}}}}{\Delta z_{j,P_{k_{min,2}}} - \Delta z_{j,P_{k_{min,1}}}}\right) \tag{9}$$

where

$$\begin{bmatrix} \left|\Delta z_{j,P_{k_{min,1}}}\right| & k_{min,1} \\ \left|\Delta z_{j,P_{k_{min,2}}}\right| & k_{min,2} \end{bmatrix} = \text{mink}\left(\ \left[\ \left|\Delta z_{j,P_1}\right|,\ \left|\Delta z_{j,P_2}\right| \cdots \left|\Delta z_{j,P_K}\right|\ \right]\ ,\ 2\ \right),\ \Delta z_{j,P_{k_{min,1}}} \cdot \Delta z_{j,P_{k_{min,2}}} < 0 \tag{10}$$

and

$$\Delta z_{j,P_k} = z_{P_k}\left(t_{det,j,P_k}\right) - z_j, \qquad z_{P_k}\left(t_{det,j,P_k}\right) = z_{P_k}^{(ref)} + \delta z_{P_k}^{(def)}\left(t_{det,j,P_k}\right) \tag{11}$$

In Eq. (10), mink([ ],2) is a Matlab function that finds the two elements of a vector [ ] that have the smallest values, and their positions $k_{min,1}$, $k_{min,2}$ in that vector.

With regard to stage A, the determination of the crossing times t_{det,j,P_k} is performed in three alternative ways in this paper:

- High-precision (HP) detection using the Simulink Hit-Crossing block, wherein Eq. (8) is solved by comparing $\theta_{P_k}\left(t_{det,j,P_k}\right)$ to θ_j and forcing increasingly smaller time steps $t_i - t_{i-1}$ in the integration of the equations of motion, until the exact detection time is determined, similarly to [3].
- Linear interpolation based on zeroing the angular difference (AD)

$$\Delta\theta_{j,P_k}(t_i) = \theta_{P_k}(t_i) - \theta_j \tag{12}$$

- Linear interpolation based on zeroing the product of angular differences (PAD) at two consecutive time steps

$$\Pi\Delta\theta_{j,P_k}(t_i) = \Delta\theta_{j,P_k}(t_i) \cdot \Delta\theta_{j,P_k}(t_{i-1}) \tag{13}$$

In either interpolation approach, for the interval $[t_{i-1}, t_i]$ to contain a crossing point, the PAD, $\Pi\Delta\theta_{j,P_k}(t_i) \le 0$ i.e.

$$\Pi\Delta\theta_{j,P_k}(t_i) \le 0 \Rightarrow t_{det,j,P_k} \in [t_{i-1}, t_i] \tag{14}$$

In either interpolation approach, the accuracy is dependent on the size of the time step $t_i - t_{i-1}$, and therefore the relative tolerance of the Matlab ODE solver. For typical integration tolerance values, AD interpolation yields BTT displacements d_j (Eq. (1)) that are very close to those obtained by the much slower high-precision (HP) crossing time approach. On the other hand, the inaccuracy of linear interpolation based on PAD is found to induce in noise-like perturbations in d_j while keeping the TOAs within the bounds of Eq. (14). As illustrated later in Section 3.3, these perturbations increase with rotational speed similarly to noise in real BTT displacement data [16–18,27]. With reference to Eq. (1), the primary source of speed-dependent noise in real displacement data is the probe's accuracy in obtaining $t_{TOA,j}$, which is quantified by its timing resolution δt_{res} [27,18]. Additional sources of error that affect the accuracy of obtaining $t_{TOA,j}$ and $t_{exp,j,P_{nom}}$ that lead to speed-dependent errors in BTT displacements include:

- sensor type (whether based on field or spot detection) [16,28];
- detection method (threshold or curve fitting) [16];
- vibration in shaft/disk leading to errors in OPR times [16];
- probe vibration in casing [17].

If the maximum magnitude of the total error from all sources is denoted as δt_{tot}, then from Eq. (1) one can express the maximum magnitude of the error in BTT displacement as

$$\delta d_j = \Omega R_{P_{nom}}^{(ref)} \delta t_{tot}, \quad \delta t_{tot} > \delta t_{res} \tag{15}$$

Eq. (15) is consistent with that in [27] (which considered δt_{res} only) and shows the increase of δd_j with both speed and blade radius.

2.3. BTT signal processing algorithm

EMTD MultiTool by Russhard [23] is a validated industrial and academic BTT software package including a BTT signal processing algorithm which processes probe TOAs into BTT amplitudes, speeds, frequencies and phases at each revolution. The software computes data preparation procedures and integral/non-integral EO data analysis based on BTT signal processing techniques in [16], which are referred to in [3] as Multi-frequency Sine Fitting with Data Preparation (MSFP). As explained in [3,16], prior to the application of BTT algorithms, a data preparation procedure is applied to the raw BTT displacement data to minimise the offset and the noise. For the present case of a single integer EO (determined from the Campbell diagram [3]), the prepared BTT displacement data d_j for a particular blade detected by N_p probes over a given revolution are given by:

$$\begin{bmatrix} d_1 \\ \vdots \\ d_{N_p} \end{bmatrix} = \begin{bmatrix} 1 & \sin(EO \times \theta_1) & \cos(EO \times \theta_1) \\ \vdots & \vdots & \vdots \\ 1 & \sin(EO \times \theta_{N_p}) & \cos(EO \times \theta_{N_p}) \end{bmatrix} \begin{bmatrix} a_0 \\ a_1 \\ a_2 \end{bmatrix} \text{ or } \mathbf{d} = \mathbf{Ba} \tag{16}$$

The vector $\mathbf{a} = [a_0 \quad a_1 \quad a_2]^T$ can then be computed, determining

A_{BTT}, ψ_{BTT} and A_{DC} at each revolution, where $A_{\mathrm{DC}} = a_0$ is the residual steady offset, the identified vibration amplitude is $A_{\mathrm{BTT}} = \sqrt{a_1^2 + a_2^2}$, and its phase is $\psi_{\mathrm{BTT}} = \tan^{-1}\left(\frac{a_2}{a_1}\right)$. From the average speed at each revolution Ω and the fixed EO, the corresponding BTT frequency f_{BTT} at a given revolution is determined as follows:

$$f_{\mathrm{BTT}} = \mathrm{EO} \times \Omega(t) \tag{17}$$

Resonance is defined to occur at the revolution for which the amplitude reaches a peak i.e. i.e. $A_{\mathrm{BTT}} = A_{\mathrm{BTT}}^{(\mathrm{peak})}$, and the corresponding frequency and speed are respectively denoted as $f_{\mathrm{BTT}} = f_{\mathrm{BTT}}^{(\mathrm{peak})}$, $\Omega = \Omega^{(\mathrm{peak})}$.

In this work, A_{BTT} and f_{BTT} will be determined from the three developed BTT simulators through two approaches for comparison:

i. applying data preparation followed by solution of Eq. (17) (all performed by EMTD MultiTool);
ii. directly solving Eq. (17) without data preparation.

The result of approach (ii) will be less accurate in the case of BTT data generated by the interpolated TOA simulators, compared to the case of BTT data generated by the high precision TOA simulator, due to interpolation errors which are akin to measurement noise.

2.4. BTT error determination

The deformation displacements of each blade's nominal sensing point P_{nom}, determined by integration of the modal equations of motion of the bladed disk assembly in a rotating frame, are used in Eq. (3) to determine $d_{\mathrm{eqv}}(t)$ at all time steps. Furthermore, all times at each integrated point are converted to rotational speed and then to frequency (given that the EO is known and fixed), i.e. $f = \mathrm{EO} \times \Omega(t)$. This is useful since it can be directly compared with $A_{\mathrm{BTT}}^{(\mathrm{peak})}$ and $f_{\mathrm{BTT}}^{(\mathrm{peak})}$. Since the TOAs and $d_{\mathrm{eqv}}(t)$ are both determined based on a mode superposition time domain solution, the error between the processed $A_{\mathrm{BTT}}^{(\mathrm{peak})}$ and $f_{\mathrm{BTT}}^{(\mathrm{peak})}$ can be directly compared with $A_{\mathrm{eqv,BTT}}^{(\mathrm{peak})}$, the resonant amplitude of $d_{\mathrm{eqv}}(t)$ (and its corresponding frequencies $f_{\mathrm{eqv,BTT}}^{(\mathrm{peak})}$). This enables the determination of the following BTT resonant amplitude and frequency errors, denoted as E_A and E_f, respectively:

$$E_A = 100 \times \left|\frac{A_{\mathrm{BTT}}^{(\mathrm{peak})} - A_{\mathrm{eqv,BTT}}^{(\mathrm{peak})}}{A_{\mathrm{eqv,BTT}}^{(\mathrm{peak})}}\right|, \tag{18}$$

$$E_f = 100 \times \left|\frac{f_{\mathrm{BTT}}^{(\mathrm{peak})} - f_{\mathrm{eqv,BTT}}^{(\mathrm{peak})}}{f_{\mathrm{eqv,BTT}}^{(\mathrm{peak})}}\right| \tag{19}$$

It is noted that the above errors are strongly dependent on the condition number (CN) of the matrix **B** (Eq. (17)) which is a measure of the sensitivity of the BTT solution, based on probe angular positions and EO [3].

3. Presentation of results and discussion

3.1. Modelling and simulation overview

The bladed disk assembly analysed in this paper is a compressor rotor from a Rolls-Royce Viper turbojet engine, shown in Fig. 2, which was dynamically tested under both non-rotational and rotational experimental conditions in [4,29]. The disk and one reference blade were 3D scanned by laser and coordinate measuring machine (CMM) respectively and the geometric models imported into *SolidWorks*. The disk and blade geometries were then exported to *ANSYS 19.2* and assembled by bonding to set up the FE model with 29 blades (shown in Fig. 2(a)) based on the reference blade, to ensure that the bladed disk assembly has identical blades. Nonetheless, the system is not perfectly tuned due to imperfect cyclical symmetry of the disk (with slight errors in CMM scanning of its features adding to this).

The engineering material properties defining the blades composed of alloy steel are as follows: density of 7640 kg/m^3; elasticity modulus of 200 GPa; Poisson's ratio of 0.28. Engineering material properties defining the disk composed of A286 Iron Base Super alloy are: density 7920 kg/m^3; elasticity modulus 190 GPa; Poisson's ratio 0.31. Modal analysis at zero rotor speed was performed on the ANSYS FE models of the individually supported blade (Fig. 2(b)) and the bladed disk assembly with identical blades (Fig. 2(a)). The meshed FE models of the individually supported blade and the bladed disk assembly have a total of 97,692 nodes (293,076 DOF) and 1698,525 nodes (5095,575 DOF), respectively. Mesh convergence was already ascertained in [4]. As previously reported [4], there are three blade-dominated mode families, associated with the respective first three modes of the individually supported blade (347.47 Hz, 1148.9 Hz, 1717 Hz). These latter modes were experimentally validated in [4] in terms of frequencies and stress-deflection ratios. The three blade-dominated families each comprise 29 members, arranged in 14 pairs with respective nodal diameter (ND) numbers 1 to 14, plus a 0 ND mode. Fig. 3 presents the natural frequencies and the ND number (N_{ND}) of each of the 29 mode members for the 1st blade dominated mode family at zero rotor speed. The average of the frequency of the $N_{\mathrm{ND}} = 14$ modes tends to correlate best with the natural frequency of the individually supported blade, as presented in Fig. 3. The 1st blade-dominated mode family is the focus of this paper. Fig. 4 presents the simulated Campbell diagram for this mode family performed from ANSYS rotordynamic analysis at four discrete speeds. It is seen that resonance is predicted at a speed of ~2500 rpm for an 8EO excitation, in line with data from an experimental rig of this bladed disk model [29]. This EO is therefore used for the simulations of

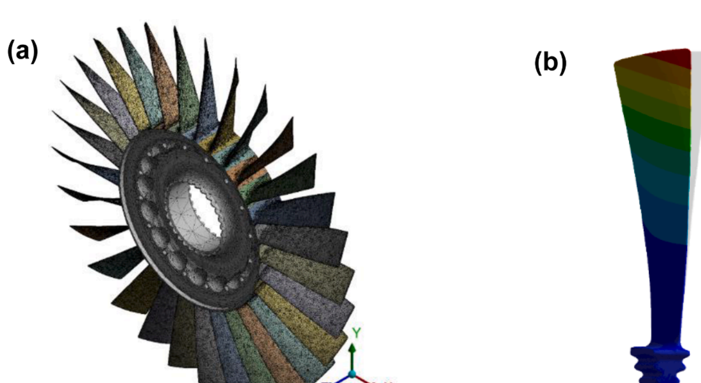

Fig. 2. (a) FE model of bladed disk assembly; (b) FE mode shape of mode no.1 of individually supported blade.

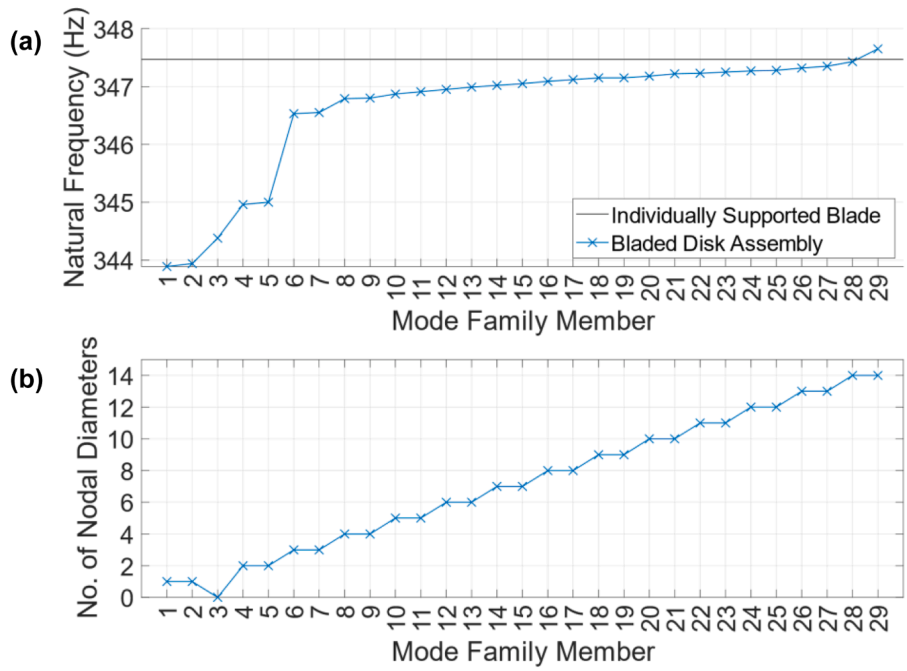

Fig. 3. FE modal analysis results for the 1st blade dominated mode family of the bladed disk assembly and the individually supported blade; (a) natural frequencies, (b) number of nodal diameters.

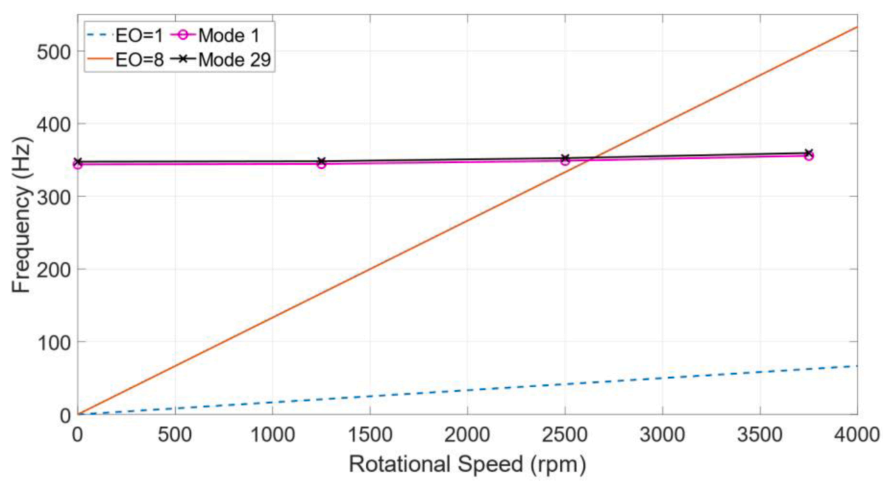

Fig. 4. Campbell diagram for the bladed disk assembly including rotational effects (centrifugal stiffening, spin softening, Coriolis).

this paper. The Campbell diagram of Fig. 4 also shows that rotation-induced inertia effects are negligible over the operational speed range of the experimental rig (0–4000 rpm), the variations in the natural frequencies of the 1st blade dominated mode family not exceeding 4% over the full range (and <1.5% at 2500 rpm).

The simulated BTT data were generated based on the parameters shown in Table 1, which correspond to the bladed disk experimental rig test of [29]. The nominal sensing position P_{nom} on all blades coincided with an FE node located 1.75 mm from the TE. A total of 9 FE nodes per blade tip, including the FE node at P_{nom} (which is the 5th FE node away from the TE), are considered in the determination of t_{det,j,P_k} in Eq. (8) i.e. $k = 1 \ldots 9$ (from which $t_{\mathrm{TOA},j}$ is then determined by axial interpolation, as per Eqs. (9)–(11)). The damping was assumed to be stiffness-proportional, with the constant β $\left(= 2\zeta_{\mathrm{exp}}/\omega_{\mathrm{exp}}\right)$ determined from estimates for damping ratio ζ_{exp} and natural frequency ω_{exp} that were in turn determined by applying the half-power point method on four experimental rig datasets. Unless otherwise stated, the travelling wave excitation in Eq. (6) is set to a phase angle corresponding to $N_{\mathrm{ND}} = 1$ to induce resonance of the $N_{\mathrm{ND}} = 1$ modes of the 1st blade-dominated mode family. The excitation on each blade was applied to the leading edge and the force amplitude was set to 2.25 N so as to result in blade tip

Table 1
Simulation parameters.

Start Speed	1000 rpm
Final Speed	4000 rpm
Total Time	130 s
Stiffness-proportional damping coefficient	9×10^{-6} s
Force amplitude $A^{(m)}_{z_{Qn}}$ (Eq. (6))	2.25 N
No. of nodal diameters N_{ND} excited (Eq. (7))	1 (unless otherwise stated)
EO (Eq. (6))	8
Probe angular positions (anticlockwise from the positive x axis in Fig. 2a)	5°, 15.15°, 23.82°, 220°, 301.5° (unless otherwise stated)
Probe axial position (z_j)	12.26 mm

peak-to-peak amplitudes of under 2.5 mm to correlate with rotational rig experimental results. The BTT data were produced with 5 probes. Unless otherwise stated, their angular positions are as shown in Table 1 so that the condition number (CN) of the matrix **B** in Eq. (16) is CN = 1.4 (the lowest possible CN for a 5-probe configuration, as determined by iterative methods in EMTD MultiTool).

A total of 145 mass-normalised modes of the undamped bladed disk assembly at zero speed were used in the time integration of the simulator's modal equations of motion (reduced order model) of the bladed disk assembly to generate the BTT data. Such a high number was not actually needed within the region of the first blade-dominated mode family (~343 Hz to ~348 Hz), but ensured convergence accuracy outside this region. This is illustrated in Fig. 5, which shows the percentage error of the results of a frequency domain (harmonic response) analysis performed using modal superposition of the first 145 modes in the frequency response functions (FRFs), compared to the full harmonic response solution (i.e. based on the FRFs computed directly from FE matrices of order 5095,575 $\times$ 5095,575). In the example shown in Fig. 5, the harmonic excitations were applied to the leading edge of each blade with $N_{\mathrm{ND}} = 0$ phasing in Eq. (7) in order to excite the corresponding mode.

3.2. Effect of axial deformation of blades on BTT data

Fig. 6 serves to validate Eq. (4). It shows the BTT displacements d_j of a particular blade as seen by one of the probes j, determined from Eq. (1) using times of arrival $t_{\mathrm{TOA},j}$ generated from the high precision simulator (Section 2.2). Also shown are $d_{\mathrm{eqv}}(t)$, its tangential component $d_{\mathrm{tang}}(t)$, and $d_{\mathrm{eqv}}(t_{\mathrm{TOA},j})$ (Eq. (4)). The close agreement of the latter with d_j confirms the validity of using $d_{\mathrm{eqv}}(t)$ (Eq. (3)) as the benchmark continuous signal for quantifying the BTT signal processing errors in Eqs. (15), (16). The significant difference between $d_{\mathrm{tang}}(t)$, and $d_{\mathrm{eqv}}(t)$ highlights the fact that the detected point on the blade is generally not the nominal sensing point. For this reason, stage B in the determination of the TOA (Section 2.2) is essential, including the use of axial interpolation between nodes on the blade tip (Eqs. (9)–(11)). The effect of the latter is illustrated in Fig. 7, which shows that picking the TOA based solely on the node with lowest $|\Delta z_{j,\mathrm{P}_k}|$ (as suggested in [3,11,13], i.e. taking $t_{\mathrm{TOA},j} = t_{\mathrm{det},j,\mathrm{P}_{k_{\mathrm{min},1}}}$ rather than axial interpolation given by Eq. (9)), results in considerable discontinuity errors in d_j, despite nine closely spaced FE nodes being considered per blade tip. The reasons why this effect was not reported in [3,11,13] are attributed to the issues raised in the penultimate paragraph of Section 1 and the final paragraph of Section 2.1.

3.3. Validation of BTT data in signal processing

3.3.1. Comparison of BTT data simulators

Fig. 8 compares the BTT data generated by the two types of interpolated TOA simulators in Section 2.2 (AD, PAD, Eqs. (9)-(10)) with the high precision (HP) TOA simulator. It is seen that the BTT displacement data from the HP TOA simulator is highly smooth (as already evident in the previous figures), providing a benchmark signal for validation of the other simulators. With the HP TOA simulator, the Simulink Hit-Crossing block forces small time-step changes in the integration of the modal equations of motion in the vicinity of a probe-node angular crossing until a highly precise $t_{\mathrm{det},j,\mathrm{P}_k}$ for each blade tip node P_k is obtained. Moreover, this process has to be repeated for each probe and as many blade tip nodes required in Eq. (8), thereby drastically increasing the simulation times with increasing numbers of probes and blades, and significant axial deformation (since this latter effect would require consideration of more nodes per blade tip in Eq. (10)). On the other hand, the simulation times required by both types of interpolated TOA simulators are not influenced by these factors and are therefore very much faster. Fig. 8 shows that the BTT displacement data from the AD-interpolated TOA simulator has only minor fluctuations arising from the interpolation error. Integration of the modal equations of motion is computed with a relative tolerance of 10^{-3} for the AD-interpolated TOA simulator. The BTT displacement data from the PAD-interpolated TOA simulator has much larger fluctuations arising from the interpolation error even when computed with a much lower relative tolerance of 10^{-9}, which results in the simulation being 4 times slower than when utilising a relative tolerance of 10^{-3}.

The maximum difference between PAD-interpolated and HP TOAs at all blades and at all revolutions is just 0.033%. However, these miniscule errors in TOAs are magnified when converted to BTT displacements (Eq. (1)), leading to speed-dependent errors in BTT displacements, strikingly similar to measurement noise e.g. [21]. The fluctuations due to errors in the PAD-interpolated data with the chosen relative tolerance of 10^{-9} amount to an average noise-to-signal ratio (NSR) of around 10%, close to NSR nominal value reported in [3,9]. Although one might consider using the much cleaner and computationally efficient AD-interpolated data with an equivalent amount of added noise, this would not yield speed-dependent errors like the PAD-interpolated TOA simulator.

Fig. 9 shows the BTT resonant amplitude error E_A (Eq. (18)) and the BTT resonant speed/frequency error E_f (Eq. (19)) at each blade using data from the PAD-interpolated TOA simulator, which was processed by the two alternative methods described at the end of Section 2.3 (i.e. using EMTD MultiTool, including data preparation, or solving directly Eq. (17) without any data preparation). The resultant mean resonant amplitude and frequencies across all blades from d_{eqv} are 2.37 mm peak-

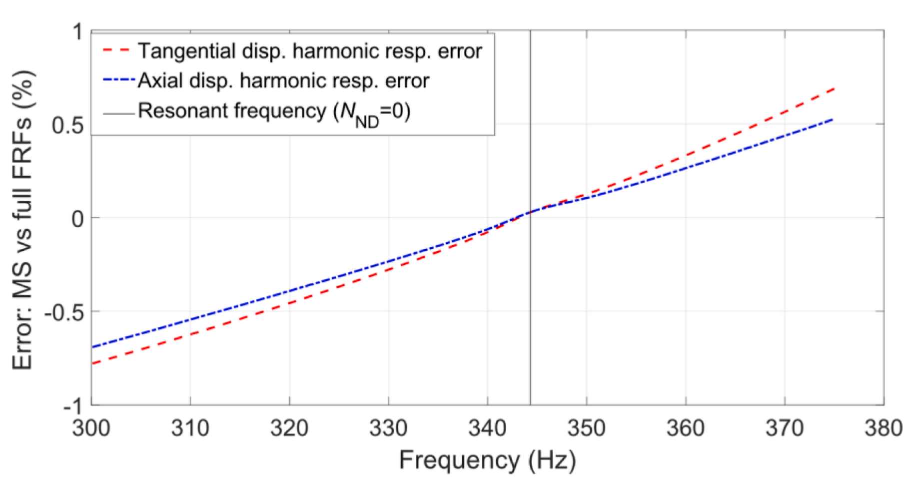

Fig. 5. Illustration of percentage error between modal superposition (MS) harmonic response solution with 145 modes and full harmonic response solution.

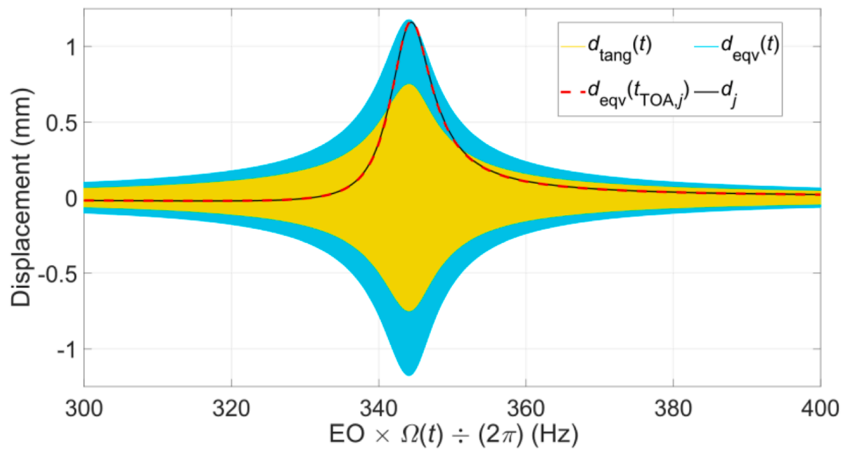

Fig. 6. BTT displacement plot between 300 and 400 Hz for blade 16 (probe 1).

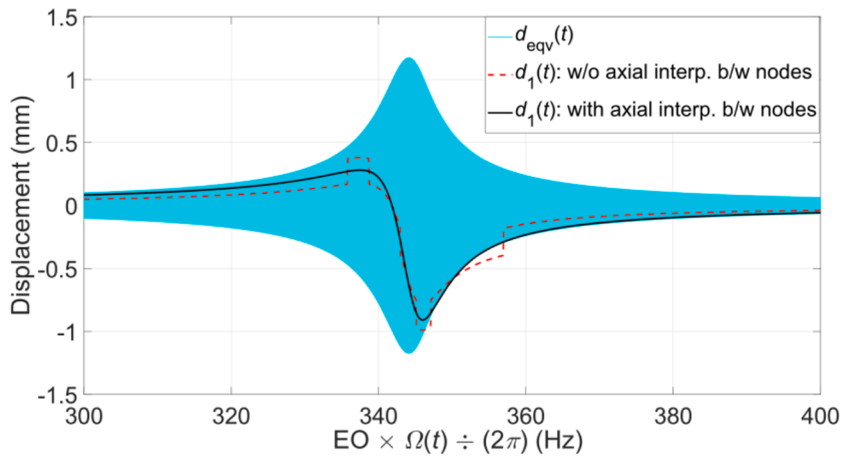

Fig. 7. Effect of axial interpolation between nodes for blade 18 (probe 1).

to-peak and 344.16 Hz, respectively. It is found that including data preparation leads to more accurate BTT amplitudes since the "noisy" BTT signal is successfully filtered, as part of the data preparation process. The maximum and average E_A across all blades decrease from 8.18% and 5.33% to 6.28% and 2.39%, respectively, when including data preparation. On the other hand, while E_f values are a fraction of a percentage by both methods, the maximum and average E_f across all blades are actually higher when including data preparation (0.29% and 0.15%) than when not including data preparation (0.27% and 0.08%). This is due to the nature of the data preparation process (e.g. filtering, averaging, etc.) applied on the under-sampled "noisy" data, which slightly hinders the identification of the resonant speed.

The above results for the PAD-interpolated TOA simulator are summarised in the "PAD" columns of Table 2, and the remaining columns of this table summarise the corresponding results for the AD-interpolated TOA simulator and the high-precision TOA simulator. It is seen that, in contrast to the PAD-interpolated TOA simulator, the BTT errors for the AD-interpolated and HP simulators increase when applying data preparation since their displacement data have negligible errors to start with. Indeed, the E_A and E_f values for the HP simulator data without data preparation can be regarded as the theoretical (minimum) errors for the used probe configuration (Table 1). The results presented in the remainder of this paper are all based on BTT data determined from the PAD-interpolated TOA simulator and processed using the commercial BTT processing software package.

3.3.2. *Identification of nodal diameter from travelling wave plot*

For each revolution, the travelling wave plot in Fig. 10 gives the Fast Fourier Transform of the BTT displacements of all 29 blades as observed by probe 1, which define a travelling wave of circular frequency equal to $(\mathrm{EO} + N_{\mathrm{ND}})\Omega$ rad/s. The plot provides a quick view to determine the nodal diameter of the resonant response (given the EO (=8) is known from the Campbell diagram), and the approximate speed and revolution at which the resonance occurs. The plot in Fig. 10 shows the correct identification of the nodal diameter of the excited mode family members. The plot also shows the increase with speed of the level of noise arising from the simulator's PAD interpolation process.

3.3.3. *Effect of condition number*

The effect of the CN is investigated to ensure the BTT data generated by the simulator conforms to previous findings from BTT data generated by a company-confidential simulator [16]. 11 potential angular positions for the probes were considered (5°, 10.6°,15.15°, 23.82°, 190.35°, 202.11°, 220°, 255.6°, 301.5°, 357°). The total number of possible combinations from the 11 aforementioned probes that make up a distinct configuration of 5 probes is 462, exhibiting CNs between 1.4 and 16.7 for an EO of 8. Fig. 11a,b investigate the effects of the CNs shown in the last column of Table 3 (corresponding to the angular positions shown) with all other parameters kept the same as in Table 1. Fig. 11a shows the variation of the maximum and mean of the resonant amplitude error across the blades ($\max(E_A)$, $\mathrm{mean}(E_A)$) and the maximum and mean values of the BTT signal processing uncertainty. This latter quantity is computed using a proprietary formula in MultiTool [23] that

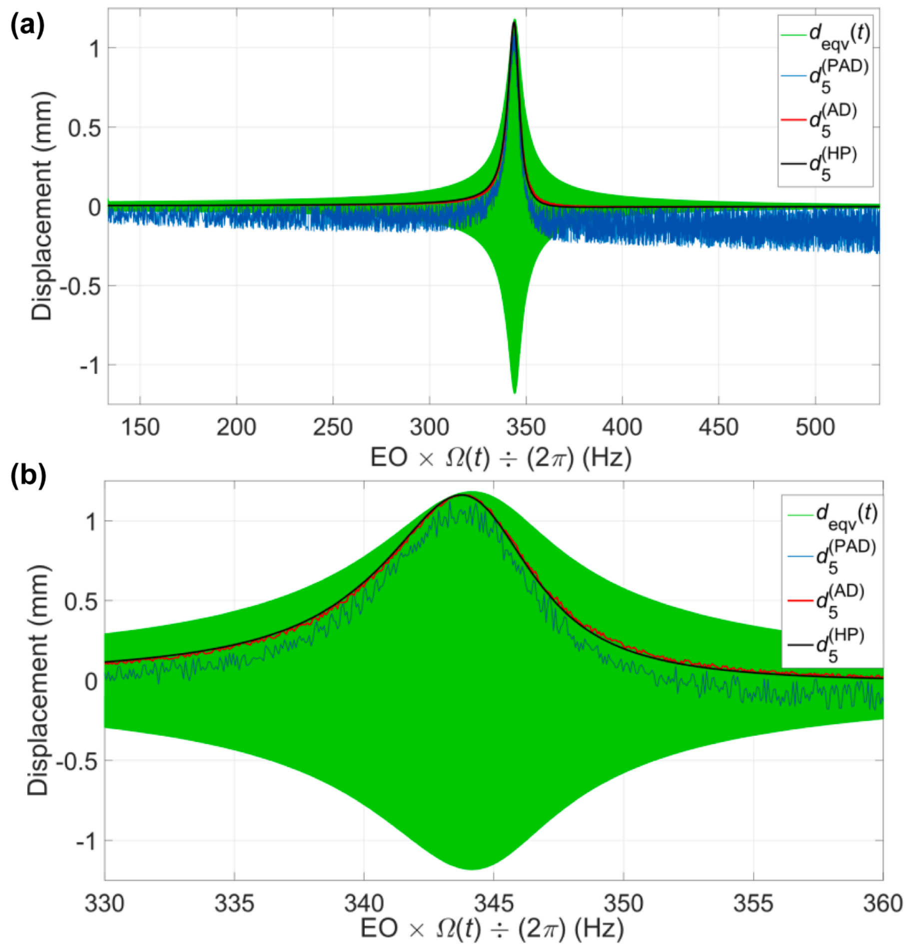

Fig. 8. Probe 5 raw BTT displacements generated by high-precision and interpolated (AD, PAD) TOA simulators $d_5^{(\mathrm{HP})}$, $d_5^{(\mathrm{AD})}$ and $d_5^{(\mathrm{PAD})}$, respectively, plotted on top of $d_{\mathrm{eqv}}(\mathrm{t})$ (blade 1): (a) wide band view; (b) zoomed view.

is not disclosed for commercial reasons [30]. However, it is described in [30] as a measure of the quality of the least squares fit (i.e. ᴅ-**Ba** in Eq. (16)). From Fig. 11a one can make the following observations.

- As the CN reduces, the overall trend in E_A and the BTT signal processing uncertainty is towards a reduction, with mean$(E_A) < 4\%$ for CN<10.
- However, a lower CN does not guarantee lower max/mean of E_A; this is consistent with the findings in [16] where it is observed that a given CN can be achieved by different configurations of a given number of probes, and the range of the mean/max BTT errors across all blades attained from these different probe configurations increases for higher CNs.
- The max/mean uncertainty graphs tend to follow the max/mean E_A graphs but the latter are essential in cases of disagreement e.g. a dip in uncertainty for CN of 7.3 is moderated by a local peak in max(E_A) of over 10%.

The latter observation is mirrored by the local peak in the maximum resonant frequency error E_f (Fig. 11b), which is nonetheless below 0.62% for all CN values considered. Although it is clear that the CN has more of an effect on E_A than E_f, it is noted that E_f is <0.31% for CNs between 1.4 and 2.6.

Further investigations involved using the aforementioned 11 potential angular positions for the probes to investigate probe configurations with different numbers of probes (ranging from 3 to 9) for the same low value of CN (CN=1.5) at an EO of 8. It was found that although convergence in mean(E_A) and mean(E_f) is evident as the number of probes is increased from 5 to 9 (reducing the likelihood of anomalies), the reduction in these values was not significant for the case studied (details of these further investigations are given in [31]).

3.3.4. Distinguishing between different ND mode responses

In the previous results, the phasing of the travelling wave excitation (Eq. (7)) was set to excite the $N_{\mathrm{ND}} = 1$ mode pairs. The final stage of the validation of the simulator is to test whether its data can enable the commercial BTT processing software to correctly distinguish between responses excited by travelling waves with N_{ND} phasing respectively corresponding to two selected mode-pair members of the 1st blade-dominated mode family. The selected mode pairs are those corresponding to $N_{\mathrm{ND}} = 1$ (frequencies of 343.89 Hz and 343.94 Hz, Fig. 3), and $N_{\mathrm{ND}} = 14$ (frequencies of 347.43 Hz and 347.65 Hz). The difference between the average frequencies of these mode pairs is therefore 1.05%. Figs. 12a,b and 13a,b shows that the BTT data from the simulator does indeed enable the BTT processing software to accurately distinguish between the two mode-pairs. In these figures, for each blade there are three values of resonant frequency (Fig. 12a,b) or resonant amplitude (Fig. 13a,b), obtained by the following alternative methods:

(i) from processing of the simulator BTT data ($f_{\mathrm{BTT}}^{(\mathrm{peak})}$, $A_{\mathrm{BTT}}^{(\mathrm{peak})}$ in Eqs. (18), (19));
(ii) from the resonant frequency and amplitude of the time history of the equivalent BTT displacement $d_{\mathrm{eqv}}(t)$ obtained from the time integrated modal solution of the simulator equations ($f_{\mathrm{eqv,BTT}}^{(\mathrm{peak})}$, $A_{\mathrm{eqv,BTT}}^{(\mathrm{peak})}$ in Eqs. (18), (19));

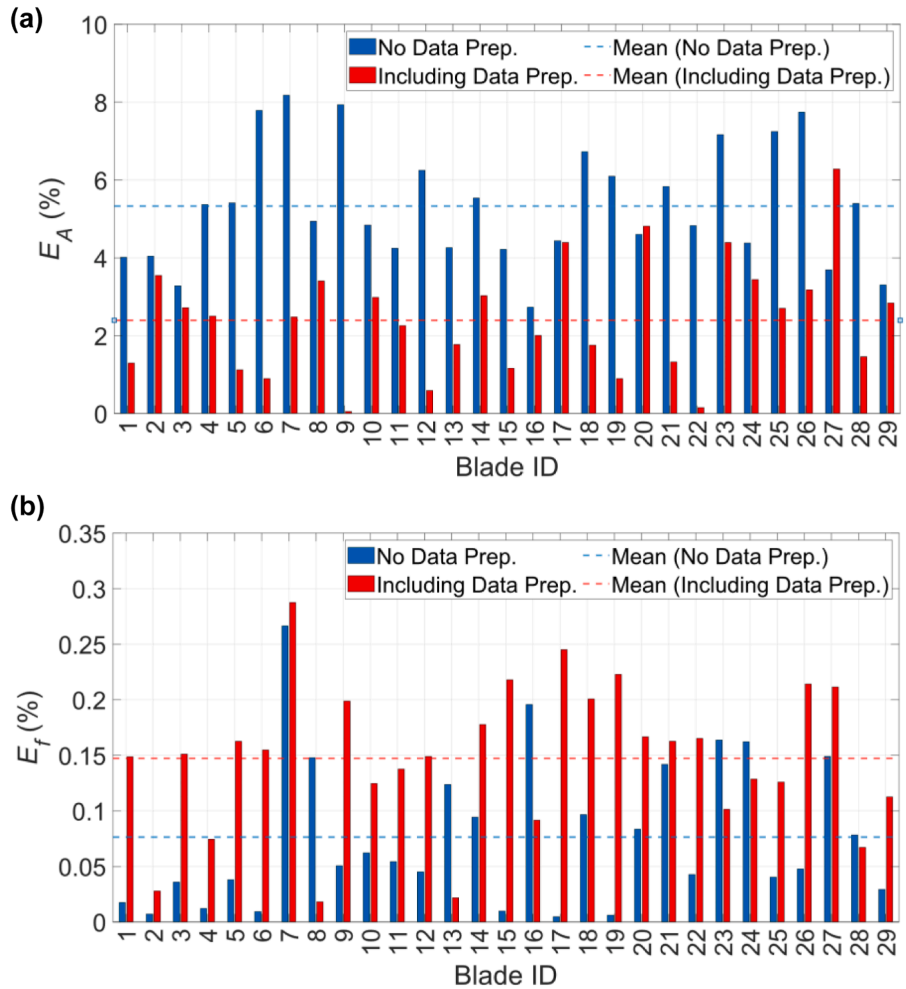

Fig. 9. Resonant amplitude error E_A (a) and resonant frequency error E_f (b) for BTT data generated by the PAD-interpolated TOA simulator for all blades.

Table 2
The maximum and average E_A and E_f across all blades of BTT data generated by the high-precision, AD-interpolated and PAD-interpolated TOA simulator, using BTT signal processing algorithm with and without data preparation.

BTT Signal Processing Method	BTT Resonant Error Type	Amplitude error E_A (%)			Frequency error E_f (%)		
	Simulator TOA Extraction Type	High-Precision	Interpolated		High-Precision	Interpolated	
			AD	PAD		AD	PAD
With Data Prep.	**Max. across all blades**	5.87	6.12	6.28	0.198	0.237	0.288
	Avg. across all blades	2.79	3.04	2.39	0.148	0.144	0.147
Without Data Prep.	**Max. across all blades**	1.28	2.02	8.18	0.0316	0.130	0.267
	Avg. across all blades	0.822	1.17	5.33	0.0201	0.0432	0.0765

(iii) from the resonant frequency and amplitude of the FRF mode superposition solution of $d_{\mathrm{eqv}}(t)$ obtained in ANSYS Workbench (wherein the simultaneous harmonic excitations on the blades are applied according to the phasing in Eq. (17) and in steps of 0.01 Hz).

The difference between the benchmark solutions (ii) and (iii) is that the latter is fully steady-state at each rpm, whereas the former is transient (acceleration of 23 rpm/s). The mean percentage difference between the resonant frequencies of Fig. 12a ($N_{\mathrm{ND}} = 1$) and Fig. 12b ($N_{\mathrm{ND}} = 14$) is 0.99% based on the BTT data (method (i)), which is the same as the difference registered by the benchmark methods (ii), (iii). The mean percentage difference between the resonant amplitudes of Fig. 13a ($N_{\mathrm{ND}} = 1$) and b ($N_{\mathrm{ND}} = 14$) is 11.62% based on BTT data (method (i)), which is very close to the differences registered by the benchmark methods (11.48% for (ii) and 11.57% for (iii)).

The reader is referred to the thesis [31] associated with this paper which contains the results of further tests showing the correct identification of simultaneously applied excitations of the same EO (8) and N_{ND} phasings of 1 and 14, respectively.

3.4. Comparison of simulated and measured BTT amplitude responses

In this penultimate section, the results for BTT amplitude-frequency response from the simulated BTT data are compared to those from the experimental rig BTT data when both types of datasets are processed by the same solver (EMTD MultiTool). The compressor rotor (bladed disk) described in Section 3.1 was instrumented and set up in the experimental rig described in [29]. Excitation was applied to the blades under rotational conditions using electromagnets adapted from [32]. Further

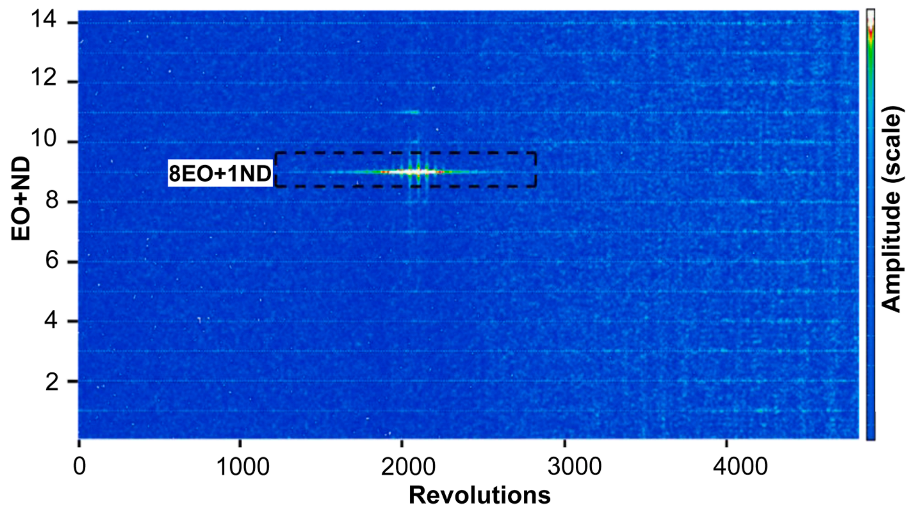

Fig. 10. Travelling wave plot (probe 1, 8EO+1ND) for PAD interpolated TOA simulator (used with integration relative tolerance of 10^{-9}).

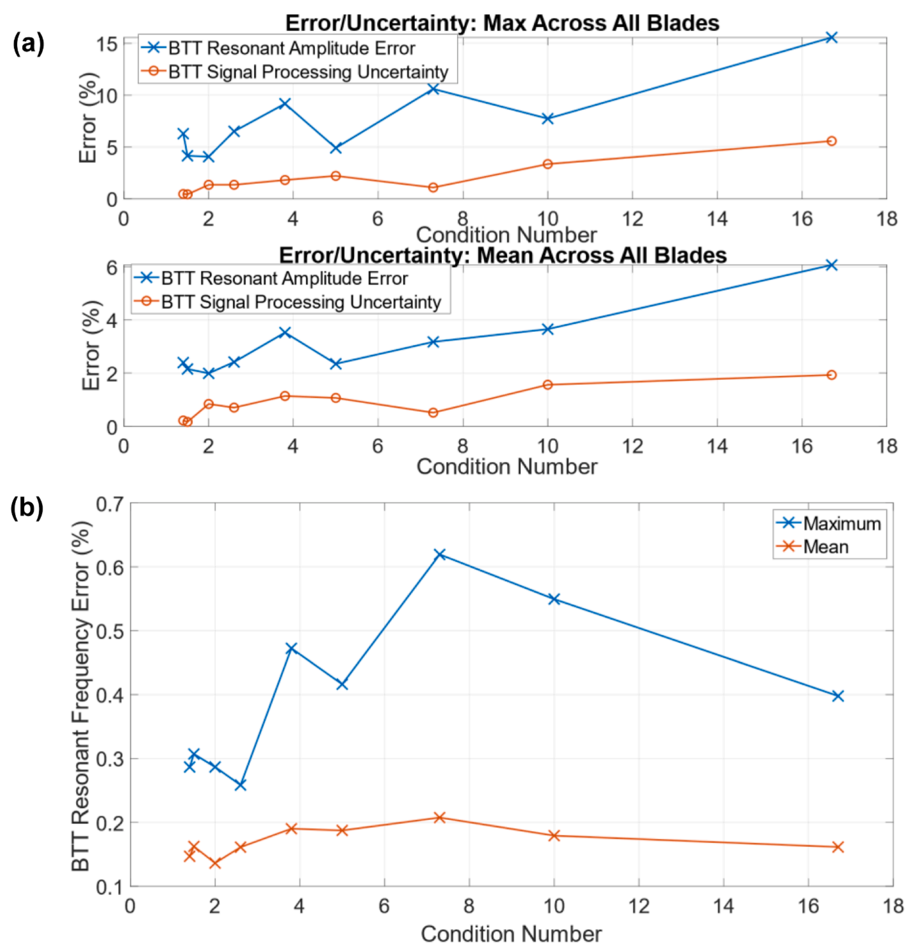

Fig. 11. Effect of condition number, for the same total number of probes (5), on BTT error: (a) maximum (upper) and mean (lower) BTT resonant amplitude error and signal processing uncertainty across blades; (b) maximum and mean BTT resonant frequency error across blades.

details on the instrumentation are found in [29]. Fig. 14a,b show examples of the best achievable correlation between the results from the simulated and experimental BTT data and Fig. 14c,d show examples of poor correlation. BTT resonant amplitudes and frequencies from the experimental data vary from 0.32 to 2.12 mm pk-pk and 326.24 and 338.85 Hz, respectively. Such large variations are not observed in the results processed from the simulated data, where BTT resonant amplitudes and frequencies merely vary from 2.20 to 2.40 mm pk-pk and 343.49 and 343.85 Hz, respectively. The FE model of the bladed disk assembly of the simulator had identical blades whose CAD model was scanned from a reference blade of the actual rotor and the low level of mistuning was due to the disk (Section 3.1). On the other hand, as noted by Mohamed et al. [4], there is variability in tip profile among the blades as a result of defects (distortions) that may have developed

Table 3
Condition number and probe positions for all probe configurations utilized.

Probe Angular Position (°)					Condition Number
Probe 1	Probe 2	Probe 3	Probe 4	Probe 5	
5	15.15	23.82	220	301.5	1.4
5	23.82	148.5	220	255.6	1.5
10.6	15.15	23.82	190.35	220	2
5	23.82	148.5	190.35	255.6	2.6
15.15	148.5	190.35	202.11	301.5	3.8
5	10.6	148.5	220	357	5
10.6	148.5	190.35	255.6	301.5	7.3
10.6	15.15	23.82	148.5	190.35	10
5	10.6	15.15	148.5	190.35	16.7

during their operating life as part of the Rolls-Royce Viper engine. Mohamed et al. [4] investigated the experimental dynamic response of 6 of the 29 blades when individually supported under non-rotating conditions, and found variations in natural frequency from 323.4 to 331 Hz. This variation is similar to the aforementioned blade-to-blade variation observed in the BTT resonant frequencies from the rotational rig, with the latter being wider (12.6 Hz compared 7.6 Hz) due to the larger number of blades in the rig (giving a wider spread of defects). Although the difference between the averages of the experimental and simulated BTT resonant frequencies is just 3%, the significant spread in blade resonant frequencies from the experimental BTT data (12.6 Hz, as opposed to a spread of just 0.4 Hz from the simulated BTT data) is indicative of a high level of mistuning that results in the considerable variability in BTT resonant amplitude. As will be shown in a later paper by the authors, such high level of mistuning also leads to difficulty in exciting a response with a specific number of NDs for a given EO since the phase angle difference between the blades would be non-uniform. In the present research, the level of mistuning in the simulator was deliberately kept minimal to enable excitation of a prescribed ND for validation on BTT processing software (Section 3.3).

Secondary sources of discrepancies between simulated and experimental results are:

- use of the OPR probe to get the expected blade arrival times for the rig – this induces errors in expected times due to vibration/noise

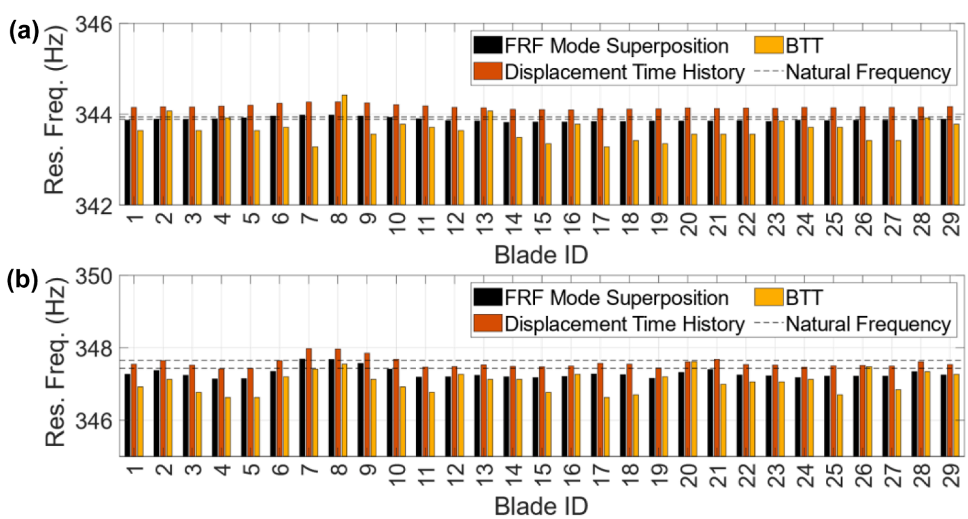

Fig. 12. Resonant frequencies generated from BTT, equivalent BTT displacement time history $d_{\mathrm{eqv}}(t)$, FRF mode superposition solution for $d_{\mathrm{eqv}}(t)$ (0.01 Hz frequency resolution), are compared for two cases, with phase set so that: (a) $N_{\mathrm{ND}} = 1$, (b) $N_{\mathrm{ND}} = 14$.

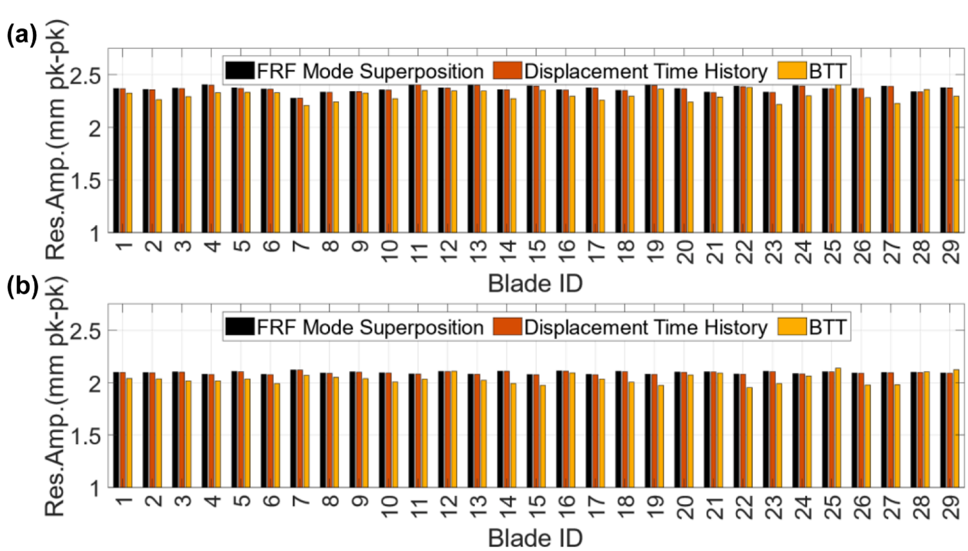

Fig. 13. Resonant amplitudes generated from BTT, equivalent BTT displacement time history $d_{\mathrm{eqv}}(t)$, FRF mode superposition solution for $d_{\mathrm{eqv}}(t)$ (0.01 Hz frequency resolution), are compared for two cases, with phase set so that: (a) $N_{\mathrm{ND}} = 1$, (b) $N_{\mathrm{ND}} = 14$.

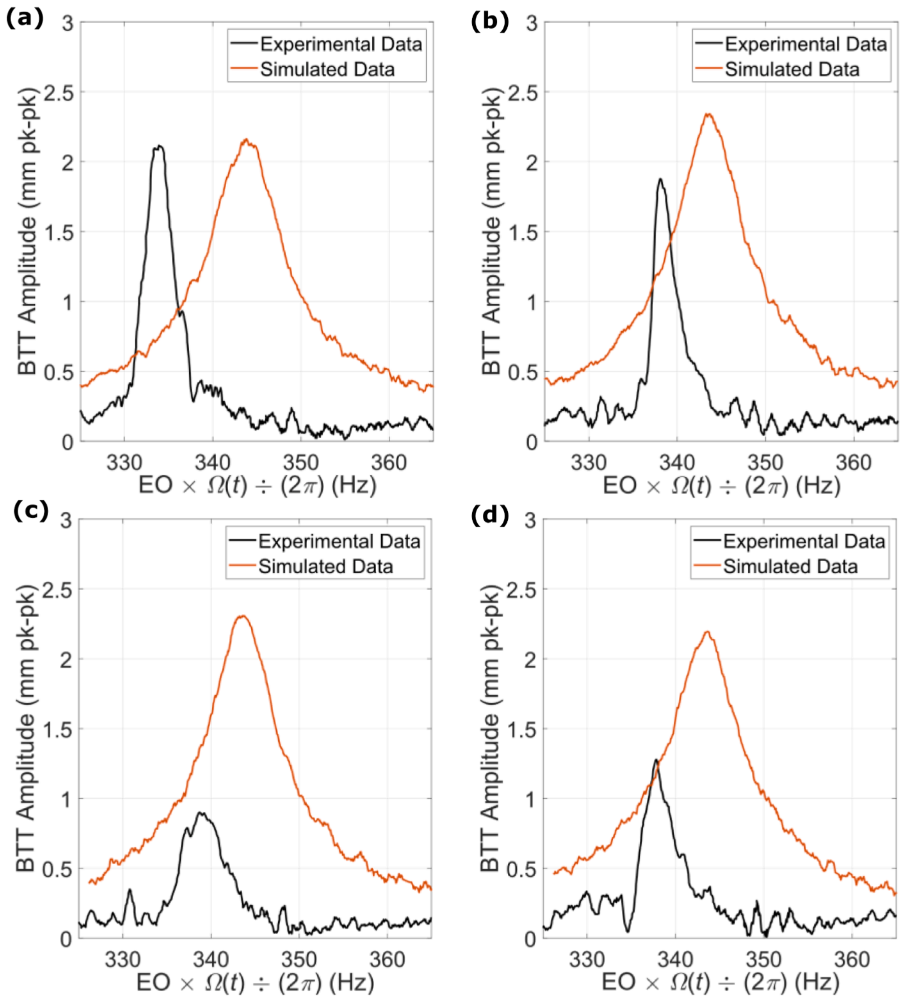

Fig. 14. BTT amplitudes (based on experimental and simulated data) across the resonant speed region: (a) blade 24; (b) blade 26; (c) blade 4; (d) blade 18.

from shaft, resulting in large speed-dependent noise induced in BTT raw displacements;

- probe positional errors;
- variable asynchronous EO excitations (due to aerodynamic effects) that were not considered in any simulations.

3.5. Discussion on the scope and limitations of the simulation study

The core innovation of the presented BTT data simulator methodology, relative to the latest simulator works e.g. [11,13], lies in the following attributes: (i) the incorporation of realistic features such as axial deformation effects on timing data and speed-dependent noise; (ii) proper alignment with the actual BTT process and independent benchmarking (as detailed in Section 2.1); (iii) the ability to handle all blades of a real aero-engine compressor stage with various probe configurations in feasible computational times; (iv) validation on an industrial-grade commercial BTT software package.

The presented simulators did not incorporate rotation-induced inertia effects (centrifugal stiffening, spin softening, Coriolis). The neglect of such effects was justified for the present study as per the Campbell diagram in Fig. 4. On the other hand, the works in [11,13] efficiently consider such effects using load interpolation [11] or matrix interpolation [13]. For studies where rotation-induced inertia effects are significant, the present modelling can be adapted according to the method presented by the co-authors in [33] for reduced order models based on zero-speed modes. It is also noted that the works in [11,13] considered noise introduced by the effect of speed fluctuation. This was out of scope of the present paper, and its inclusion would likely hinder observation of speed dependent errors.

The present study investigated the optimisation of the configuration of a set of 5 probes, and further studies in [31] consider sets of 3 to 9 probes (finding that a minimum of 5 probes is satisfactory). Such numbers are typical for the industrial BTT processing software used. It is noted that researchers in [34] have developed an algorithm aimed at reducing the number of probes to 2. However, the potential savings in installation costs of such a system need to be weighed against its increased vulnerability to downtime in the event of one of the probes failing in the harsh environment.

As in [11,13], the excitations in the present paper were limited to integer EOs, although the signal processing method used can handle asynchronous excitations [3]. Asynchronous excitation introduces fluctuations in BTT data [3] that obscure the speed-dependent noise and was therefore not useful for the purpose of this research.

The investigation of mistuning was not within the scope of the present study, and the level of mistuning in the simulator model was kept minimal (by using identical blades) to facilitate excitation of a response with a specific number of NDs (as explained towards the end of the first paragraph of Section 3.4). However, the model can accurately accommodate any level of stiffness or mass mistuning of the blades since the modes of the actual (mistuned) assembly are used in the modal superposition for the vibration response (in fact, the slight geometric asymmetry in the scanned disk model is captured in the present model as reflected in the slight blade-to-blade variability of the benchmark results in Figs. 12 and 13). On the other hand, the works in [11,13] use an alternative approach based on the component mode mistuning method. In this approach, the vibration response for small mistuning in the blades is obtained from the modal superposition of the modes of the tuned bladed disk assembly, with the mistuning effect accounted in the modal coordinates' equation of motion by additional terms for each blade that are weighted by mistuning parameters and reduced using the modes of a representative cantilevered blade. This approach of [11,13] has the advantage of enabling more efficient analysis of different mistuning configurations and facilitates experimental model updating of the individual blades' mistuning levels. It also allows the investigation of variability in damping from blade to blade (damping mistuning), which cannot readily be accommodated in the present form of the reduced order model of the present paper.

4. Conclusions

This paper has presented three novel bladed disk simulators for BTT data based on a finite element modal model. The data have been validated in a novel type of study that considered all blades of an aero-engine compressor, and which used an industrial-grade commercial BTT software package to identify an excited blade mode-family member from the data. The simulators differed with regard to the method used for the determination of the blade-probe crossing times in the circumferential direction: high precision (HP) using successive time-step reduction; time-step interpolation based on either angular difference (AD) relative to the probes, or the product of angular difference (PAD). All three used the same novel axial interpolation method to determine the correct time of arrival (TOA) from the aforementioned times taking into account deviations from the nominal sensing position on the blade tip (P_{nom}) caused by axial deformation.

The main findings are summarised as follows:

i. An introduced equivalent BTT displacement function based on P_{nom} has been proven to be a valid benchmark for validating both BTT displacement data and the processed amplitude and frequency.
ii. The use of axial interpolation for the TOA eliminated errors due to discontinuities in BTT displacement data caused by discrete FE nodes on the blade tips.
iii. The interpolated TOA simulators (AD, PAD) enabled the generation of BTT data from all blades and probes within feasible time frames.
iv. Whereas the AD-interpolated TOA simulator had a comparable accuracy to the HP TOA simulator, the PAD-interpolated TOA simulator induced speed-dependent errors in the BTT displacement data analogous to measurement noise caused by probe timing errors.
v. Such errors, amounting to an average noise-to-signal ratio of 10%, were successfully processed by the BTT software, resulting in mean errors in resonant amplitude and frequency of 2.4%, 0.15%, respectively, and correct identification of the ND by the travelling wave plot.
vi. The effect of the probe configuration condition number on the simulated BTT data was shown to be consistent with established findings, and the resonant amplitude error criterion based on (i) above was shown to be consistent with (and complementary to) the proprietary uncertainty parameter used in the commercial BTT processing software.
vii. The simulated BTT data were shown to correctly distinguish between two excited mode-pair members of a mode-family whose natural frequencies differed by just 1%.
viii. Although the blade resonant frequencies identified from the simulated BTT data differed by just 3% on average from those identified from experimental BTT data, the simulator did not capture the significant variability in frequency and amplitude observed across the blades of the experimental rig since its model was based on identical blades.

Having validated the simulated BTT data on BTT processing software, a future paper will consider the effect of mistuning from blade mass variability on the simulated BTT data and the processed resonant amplitude, frequency and stress-deflection ratios.

Data statement

The data that support the findings of this study are available from the corresponding author upon reasonable written request.

CRediT authorship contribution statement

Alhassan Nour: Writing – review & editing, Writing – original draft, Visualization, Validation, Software, Methodology, Investigation, Formal analysis, Conceptualization. **Philip Bonello:** Writing – review & editing, Writing – original draft, Supervision, Software, Resources, Project administration, Methodology, Funding acquisition, Data curation, Conceptualization. **Peter Russhard:** Validation, Software, Methodology. **Mohamed Elsayed Mohamed:** Writing – review & editing, Software, Methodology. **Pavel Procházka:** Writing – review & editing, Validation. **Mohammed Lamine Mekhalfia:** Writing – review & editing, Validation.

Declaration of competing interest

The authors declare the following financial interests/personal relationships which may be considered as potential competing interests:

Alhassan Nour reports financial support was provided by Engineering and Physical Sciences Research Council. If there are other authors, they declare that they have no known competing financial interests or personal relationships that could have appeared to influence the work reported in this paper.

Acknowledgment

The authors acknowledge the Engineering and Physical Sciences Research Council (EPSRC) for its financial support of Dr A. Nour's PhD project (Training Grant EP/T517823/1, project reference 2373190), and the European Commission (Horizon 2020 Project Batista, Grant Agreement ID: 862034) for the provision of experimental data.

Data availability

Data will be made available on request.

References

[1] P. Russhard, The rise and fall of the rotor blade strain gauge, in: J.K. Sinha (Ed.), Proceedings of VETOMAC X 2014, Mechanisms and Machine Science, Proceedings of VETOMAC X 2014, Mechanisms and Machine Science, 23, Springer International Publishing, Switzerland, 2015, pp. 27–37.
[2] F. Wang, C. Fu, S. Tian, J. Liu, L. Zheng, Blade tip timing-based blade vibration measurement technology and its applications to aeroengine: a systematic review, Aerosp. Sci. Technol. 168 (2026) 111064, https://doi.org/10.1016/j.ast.2025.111064, 111064.
[3] M.E. Mohamed, P. Bonello, P. Russhard, An experimentally validated modal model simulator for the assessment of different blade tip timing algorithms, Mech. Syst. Signal Process. 136 (2020) 106484, https://doi.org/10.1016/j.ymssp.2019.106484, 106484.
[4] M.E. Mohamed, P. Bonello, P. Russhard, P. Procházka, M.L. Mekhalfia, E.B. T. Tchuisseu, Experimental validation of FEM-computed stress to tip deflection ratios of aero-engine compressor blade vibration modes and quantification of associated uncertainties, Mech. Syst. Signal Process. 178 (2022) 109257, https://doi.org/10.1016/j.ymssp.2022.109257, 109257.
[5] A. Nour, P. Bonello, M.E. Mohamed, P. Russhard, P. Procházka, M.L. Mekhalfia, Towards accurate error determination in blade tip timing data generated by a novel bladed disk modal model simulator, in: Proceedings of the 13th Conference on

Vibrations in Rotating Machinery (VIRM 13), One Birdcage Walk, London, 2025, 16-18 Septemberin press.
[6] I.B. Carrington, J.R. Wright, J.E. Cooper, G. Dimitriadis, A comparison of blade tip timing data analysis methods, Proc. Inst. Mech. Eng. Part G J. Aerosp. Eng. 215 (5) (2001) 301–312, https://doi.org/10.1243/0954410011533293.
[7] G. Dimitriadis, I.B. Carrington, J.R. Wright, J.E. Cooper, Blade-tip timing measurement of synchronous vibrations of rotating bladed assemblies, Mech. Syst. Signal Process 16 (2002) 599–622, https://doi.org/10.1006/mssp.2002.1489.
[8] J. Gallego-Garrido, G. Dimitriadis, J.R. Wright, Development of a multiple modes simulator of rotating bladed assemblies for blade tip-timing data analysis, in: P. Sas, B. Van Hal (Eds.), Proceedings of the International Conference on Noise and Vibration Engineering, Heverlee, Belgium, Katholieke Universiteit Leuven, 2002, pp. 1437–1446.
[9] J. Gallego-Garrido, G. Dimitriadis, J.R. Wright, A class of methods for the analysis of blade tip timing data from bladed assemblies undergoing simultaneous resonances—Part I: theoretical development, Int. J. Rotating Mach. 2007 (2007) 1–11, https://doi.org/10.1155/2007/27247, 27247.
[10] Z. Liu et al., Blade tip-timing measurement mathematical modeling and simulation without OPR under the condition of rotating speed fluctuation, in: Reliability and Prognostics and Health Management (PHM-Nanjing), 2021 Global, 2021, pp. 1–6.
[11] D. Wei, H. Li, Y. Chen, H. Cao, Z. Fan, Y. Li, Development of blade tip timing signal simulator based on a novel model reduction method of bladed disks, J. Sound Vib. 534 (2022) 117053, https://doi.org/10.1016/j.jsv.2022.117053, 117053.
[12] F. Figaschewsky, B. Hanschke, A. Kühhorn, Efficient generation of engine representative tip timing data based on a reduced order model for bladed rotors, J. Eng. Gas Turbines Power 141 (1) (2019) 012503, https://doi.org/10.1115/1.4040748.
[13] C. Wang, H. Li, Y. Chen, H. Cao, Y. Zhang, X. Zhao, A novel blade tip timing data generation method based on the enhanced reduced-order model, Aerosp. Sci. Technol. 169 (2026) 111433, https://doi.org/10.1016/j.ast.2025.111433, 111433.
[14] I.B. Carrington, D. Dimitriadis, J.R. Wright, J.E. Cooper, et al., A comparison of blade tip timing data analysis methods, in: A.G. Starr, et al. (Eds.), Proceedings of the DYMAC 99 - 1st International Conference on the Integration of Dynamics, Monitoring and Control for the 21st century, Manchester, 1999.
[15] M. Mohamed, P. Bonello, P. Russhard, A novel method for the determination of the change in blade tip timing probe sensing position due to steady movements, Mech. Syst. Signal Process 126 (2019) 686–710, https://doi.org/10.1016/j.ymssp.2019.02.016.
[16] P. Russhard, Development of a Blade Tip Timing Based Engine Health Monitoring System, The University of Manchester, Manchester, United Kingdom, 2010. Eng.D. thesis.
[17] C. He, J. Antoni, A.P. Daga, H. Li, N. Chu, S. Lu, Z. Li, An improved key-phase-free blade tip-timing technique for nonstationary test conditions and its application on large-scale centrifugal compressor blades, IEEE Trans. Instrum. Meas. 70 (2021) 1–16, https://doi.org/10.1109/TIM.2020.3033463, 3504516.
[18] R. Przysowa, J. Spychała, Health monitoring of turbomachinery based on blade tip-timing and tip-clearance, in: Proceedings of the RTO AVT Symposium on Ensured Military Platform Availability, RTO-MP-AVT-157, Montreal, Canada, NATO Research and Technology Organisation (RTO), 2008, https://doi.org/10.14339/RTO-MP-AVT-157-14-pdf.
[19] W. Wang, X. Zhang, D. Hu, D. Zhang, P. Allaire, A novel none once per revolution blade tip timing based blade vibration parameters identification method, Chin. J. Aeronaut. 33 (2020) 1953–1968, https://doi.org/10.1016/j.cja.2020.01.014.
[20] S. Ren, X. Xiang, W. Zhao, Q. Zhao, C. Wang, Q. Xu, An error correction blade tip-timing method to improve the measured accuracy of blade vibration displacement during unstable rotation speed, Mech. Syst. Signal Process 162 (2022) 108030, https://doi.org/10.1016/j.ymssp.2021.108030, 108030.
[21] W. Wang, K. Chen, X. Zhang, W. Li, A novel method to improve the precision of BTT under rapid speed fluctuation conditions, Mech. Syst. Signal Process 177 (2022) 109203, https://doi.org/10.1016/j.ymssp.2022.109203, 109203.
[22] A. Savitzky, M.J.E. Golay, Smoothing and differentiation of data by simplified least squares procedures, Anal. Chem. 36 (1964) 1627–1639.
[23] P. Russhard, MultiTool Blade Tip Timing Acquisition, Analysis and Data Simulation Software v4.5.12 [Software], EMTD Ltd., Nottingham, UK, 2025.
[24] M.E. Mohamed, Towards Reliable and Efficient Calibration of Blade Tip Timing Measurements Against Finite Element Model Predictions, The University of Manchester, Manchester, United Kingdom, 2019. Ph.D. Thesis.
[25] F. Nyssen, R. Viguié, D. Simon, J.C. Golinval, A methodology for the appropriation and the isolation of nodal diameter modes in cyclic symmetric structures, in: Proceedings of the ASME 2013 International Design Engineering Technical Conferences and Computers and Information in Engineering Conference, 2013, https://doi.org/10.1115/DETC2013-12919 paper no: DETC2013-12919, V008T13A012.
[26] P. Russhard, Derived once per rev signal generation for blade tip timing systems, in: Proceedings of the IET Conference Proceedings, The Institution of Engineering & Technology, 2014, https://doi.org/10.1049/cp.2014.0551.
[27] H. Li, S. Wu, Z. Yang, R. Yan, X. Chen, Measurement methodology: blade tip timing: a non-contact blade vibration measurement method, IEEE Instrum. Meas. Mag. 26 (2023) 12–20, https://doi.org/10.1109/MIM.2023.10328672.
[28] O. Jousselin, Development of Blade Tip Timing Techniques in Turbo Machinery, The University of Manchester, Manchester, United Kingdom, 2013. Eng.D. Thesis.
[29] CORDIS - EU research results, Blade tip timing system validator (Batista), horizon 2020, Grant Agreement ID: 862034. 10.3030/862034, 2021 (accessed 26 November 2025).
[30] R. Przysowa, P. Russhard, Non-contact measurement of blade vibration in an axial compressor, Sensors 20 (2019) 68, https://doi.org/10.3390/s20010068.
[31] A. Nour, Development of Blade Tip Timing Simulation Tools Based on A Finite Element Modal Model, The University of Manchester, Manchester, United Kingdom, 2025. Ph.D. Thesisavailable from September 2026.
[32] M.L. Mekhalfia, P. Procházka, R. Smid, P. Bonello, P. Russhard, D. Maturkanic, M. E. Mohamed, E.B.T. Tchuisseu, Electromagnetic excitation for blade vibration analysis in static conditions: theoretical insights and experimental evaluation, IEEE Trans. Instrum. Meas. 73 (2024) 1–8, https://doi.org/10.1109/TIM.2024.3488153, 6011008.
[33] D. Wei, H. Li, Y. Chen, H. Cao, Z. Fan, Y. Li, Development of blade tip timing signal simulator based on a novel model reduction method of bladed disks, J. Sound Vib. 534 (2022) 117053, https://doi.org/10.1016/j.jsv.2022.117053, 117053.
[34] Z. Fan, H. Li, J. Dong, X. Zhao, D. Wei, Q. Zhou, Blade vibration difference-based identification of blade vibration parameters: a novel blade tip timing method, J. Sound Vib. 512 (2021) 116402, https://doi.org/10.1016/j.jsv.2021.116402, 116402.